RSC Advances

PAPER

High sensitivity glucose detection at extremely low concentrations using a MoS$_2$-based field-effect transistor

Junjie Shan,[a] Jinhua Li, [ID]*[a] Xueying Chu,[a] Mingze Xu,[a] Fangjun Jin,[a] Xiaojun Wang,[b] Li Ma,[b] Xuan Fang,[ac] Zhipeng Wei[c] and Xiaohua Wang[c]

In recent years, molybdenum disulfide (MoS$_2$) based field-effect transistors (FETs) have attracted much attention because of the unique properties of MoS$_2$ nano-materials as an ideal channel material. Using a MoS$_2$ FET as a glucose solution biosensor has the advantages of high sensitivity and rapid response. This paper is concerned with the fabrication of a bilayer MoS$_2$-based FET and the study of its application in the high sensitivity detection of an extremely low concentration glucose solution. It was found that the source-drain current (I_{ds}) increases as the concentration of the glucose solution increases at the same gate voltage (V_{gs}) and drain voltage (V_{ds}). The sensitivity of the biosensor as high as 260.75 mA mM^{-1} has been calculated and the detection limit of 300 nM was measured. The unknown concentration of a glucose solution was also detected using data based on the relationship between I_{ds} and glucose solution concentration. In addition, many significant advantages of the biosensor were observed, such as short response time (<1 s), good stability, wide linear detection range (300 nM to 30 mM) and the micro-detection of glucose solutions. These unique properties make the bilayer MoS$_2$-based FET a great potential candidate for next generation biosensors.

Introduction

FETs are an important part of modern microelectronic technology for the advantages of high input resistance, low noise, low power consumption, large dynamic range, easy integration, non secondary breakdown phenomenon and wide safe working range. The main applications of FETs are in amplified circuits, impedance conversion, variable resistance, constant current sources, electronic switches and so on. MoS$_2$ is an ideal channel material for FETs due to the small number of dangling bonds on the surface of MoS$_2$ and its stable structure.[1–8] FETs based on MoS$_2$ have the advantages of high switching current ratio, high carrier mobility and low energy dissipation, which meet the requirements of smaller size, lower cost, less power consumption, and faster computing in integrated circuits for modern electronic products.[7,8] Applications of MoS$_2$ FETs in novel electronic devices such as electrochemical sensors, biosensors, solar cells, and gas sensors, have recently been reported.[9,10]

In recent years, the sensors based on MoS$_2$ FETs have been developed to detect various species such as H$_2$O$_2$, NO$_2$, NH$_3$,

DNA, proteins and so on. These devices have attracted huge interest because of the advantages such as high sensitivity, low detection limit, label free detection, low power consumption, portability and large scale production.[9,11–17] The sensor and the test system can also be integrated on a chip to actualize the macroscopic and fast detection of the measuring object.[9,18] Relevant research shows that the sensitivity of a MoS$_2$-based pH sensor has been achieved as high as 59 mV per pH. Ultrasensitive and specific protein sensing has also been achieved with a sensitivity of 196 mV per pH even at 100 femtomolar concentration.[11] Zhou and his group have demonstrated the good sensing performance of the MoS$_2$ FET towards nitrogen dioxide (NO$_2$) and ammonia (NH$_3$).[9,19]

Some of the salient features of 2D layered MoS$_2$ for different sensing applications have been researched, including the biosensing, gas sensing, electrochemical sensing and SERS sensing.[9] Due to the wide application of sensitive and reliable glucose sensing in clinical diagnosis, food analysis and biotechnology, the development of glucose sensor has received continuous interest.[20] The detection of glucose in blood and cells will be significant for medical study.[21] Currently, the electrochemistry method is mainly used for the detection of glucose concentration.[22–25] But this method requires the environment containing a large amount of liquid, which leads the activity of biological protein molecules to be affected seriously by temperature, toxicity and pH value of the environmental. The microdetection of glucose solution cannot be achieved accurately and the detection process is cumbersome and lacks stability.

School of Science, International Joint Research Center for Nanophotonics and Biophotonics, Changchun University of Science and Technology, 7089 Wei-Xing Road, Changchun 130022, P. R. China. E-mail: jhli_cust@163.com; Tel: +86 0431 85582739

Department of Physics, Georgia Southern University, Statesboro, GA 30460, USA

State Key Laboratory of High Power Semiconductor Laser, Changchun University of Science and Technology, 7186 Wei-Xing Road, Changchun 130028, P. R. China

At recent reports, FET based glucose biosensor have been successfully prepared by different channel materials, such as carbon nanotubes, ZnO and graphene. The biosensor based on graphene FET has a narrow linear range (3.3–10.9 mM).[26] The linear range can be broadened to a large extent when the channel material is replaced by carbon nanotubes or ZnO.[27,28] But their long response time of ~10 s is not conducive to the rapid and accurate concentration detection of glucose solution. On the other hand, researchers have corroborated through theoretical and experimental studies that the zero band gap of graphene limits its application in semiconductor devices.[11] Contrast to graphene, the MoS_2 which has the similar layered structure to graphene shows better promising properties for biosensors due to its non-zero band gap.[3,9,29–34] The layered MoS_2 nanomaterial have been recently developed and employed in various applications, including some new sensors because of it layer-dependent electrical properties.[9] In previous studies, Li *et al.* reported the observation of thickness reduction induced crossover of electrical contact at Au/MoS_2 interfaces.[35] They found that the interfacial potential barrier can be finely tailored from 0.3 to 0.6 eV by merely varying the thickness of MoS_2. The contact resistivity of devices slightly decreases with the reducing of MoS_2 thickness, which mainly governed by the quantum confinement effect.[35] In addition, the density of states of bilayer MoS_2 nanosheet is three times higher than that of monolayer MoS_2, leading to considerably high drive currents in the ballistic limit. The conducting channels can be created by field effect in bilayer MoS_2 for boosting the current drive of FETs.[36] Moreover, the Hall mobilities increase as the density of states increases, reaching 375 cm^2 V^{-1} s^{-1} for the bilayer, in contrast to 250 cm^2 V^{-1} s^{-1} for the monolayer.[37] Therefore, the bilayer MoS_2 FET based biosensor would exhibits the stable and high sensitive responses due to the strong impact of its structure and electrical properties.[38] Unfortunately, the detection of glucose solution based on the MoS_2 FET has not been reported so far. In our research, a biosensor based on the bilayer MoS_2 back-gate FET was fabricated successfully and the application of the biosensor in detection of glucose concentration was demonstrated for the first time. We discovered that the I_{ds} of the biosensor increases with the increase of glucose concentration. Through the measurements of I_{ds}, the MoS_2 FET biosensor shown a good sensing performance. The high sensitivity of 260.75 mA mM^{-1} and extremely low detection limit of 300 nM have been achieved in our researches.

Experimental section

Materials and reagents

MoS_2 bulk materials (Spi, SUPPLIES), D-glucose ($C_6H_{12}O_6 \cdot H_2O$, 99.5%), Glucose oxidase (GOx, from *Aspergillus niger* species, 180 U mg^{-1}). Potassium phosphate monobasic (KH_2PO_4, 99.5%), potassium phosphate dibasic trihydrate ($K_2HPO_4 \cdot 3H_2O$, 99.0%), potassium hexacyanoferrate ($K_3[Fe(CN)_6]$), potassium ferrocyanide ($K_4[Fe(CN)_6] \cdot 3H_2O$).
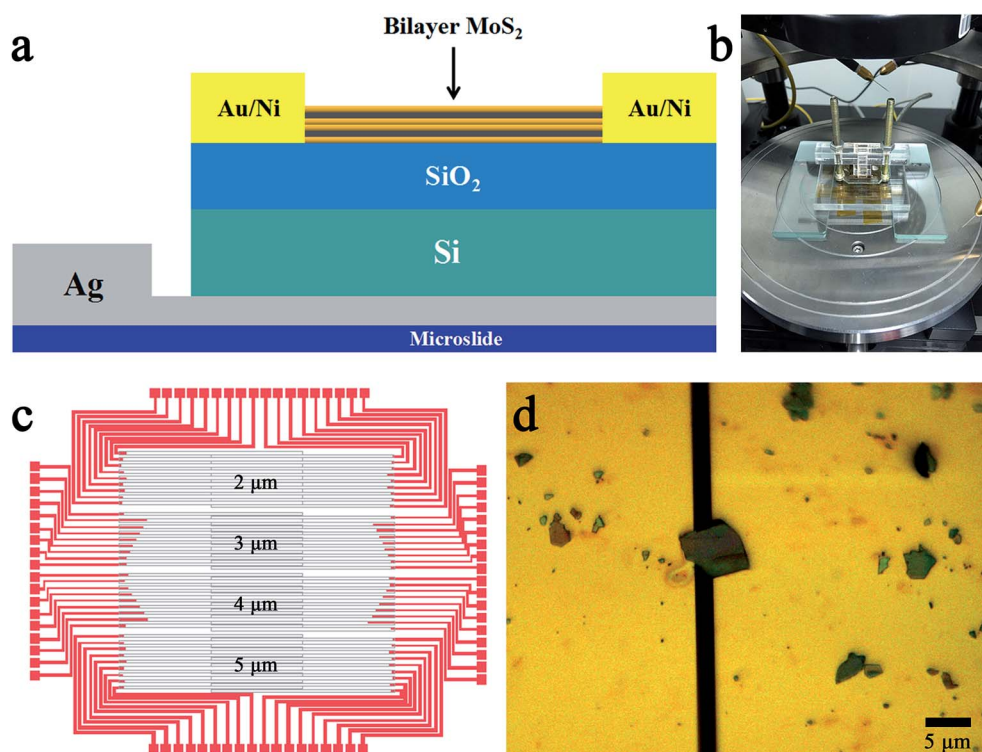

Fig. 1 MoS_2-based FET biosensor device. (a) Schematic diagram of the bilayer MoS_2-based FET. (b) Optical image of the sample cell. The glucose solution is injected into the rectangular hole of the sample cell. (c) Image of the lithography board. Four kinds of devices with different channel widths, 2, 3, 4 and 5 μm, are included in the board. (d) The metallographic micrograph of the channel material stripped mechanically in the channel region of (c). The length and width of the MoS_2 channel are 2 and 3 μm, respectively.

The specific preparation process of the glucose solution with different concentrations is as follows: 80 mL of a 0.1 mol L^{-1} PBS solution was prepared as the solvent for the glucose solution, the PBS is a mixture of KH_2PO_4, K_2HPO_4, $K_3Fe(CN)_6$, and $K_4Fe(CN)_6$. The glucose of different quality was dissolved in PBS solution to guarantee the concentration of glucose solution as 0–30 mM. Appropriate amounts of glucose oxidase (GOx) was added to each glucose solution before testing.

Fabrication of FET based glucose biosensors

In our study, the different concentration of glucose solution was detected by a FET biosensor. The back-gate FET was adopted due to the surface of channel material had to contact with the glucose solution in the sensing process. The structure of the MoS_2 FET is shown in Fig. 1a. In addition to the FET, a sample cell was also necessary. The sample cell which made of plexiglass was designed to three parts and screwed together with the MoS_2 FET. The physical diagram of the sample cell is shown in Fig. 1b. In the process of testing, the glucose solution with different concentration was injected into the rectangular hole which above the sample cell. In order to protect the channel material, electrodes of the back-gate FET was formed on the SiO_2/Si substrate which before the MoS_2 was exfoliated. The source and drain electrodes were made of Au/Ni (70 nm/10 nm), and the back gate electrode was made of quick-dry silver paste. The device was placed on a square glass plate (1.5 cm × 1.5 cm) and the back-gate electrode was leaded to the glass plate. The specific process is as follows:

The first process is to design the board of the UV photolithography which was used to prepare the source and drain electrodes of MoS_2 FET, as shown in Fig. 1c. The overlapping areas of the gray electrode leads are the channel regions of the FET. The channel width of the MoS_2 FET was designed to 2, 3, 4 and 5 μm, respectively. The preparation of the electrodes were carried out by the UV photolithography technique and the electron beam (e-beam) evaporation technique on the SiO_2/Si substrate. The next procedure is to exfoliate the highly mirrored MoS_2 bulk materials in channel regions, which was shown in Fig. 1c. Micromechanical exfoliation (Scotch-tape method) is the traditional and the simplest technique used for the preparation of atomically thin layered 2D nanomaterials with high quality and crystallinity.[9] This technology is widely used in preparation of the channel materials of FETs. Metallographic micrograph of the channel material was shown in Fig. 1d, the yellow parts were the source and drain electrode leads formed by the e-beam deposition of 70 nm/10 nm Au/Ni, and the black regions between the lead wires were the channel regions. The length and width of the MoS_2 channel material we prepared are 2 and 3 μm, respectively. Subsequent characterizations and tests are all performed on this device. The final step is the preparation of back-gate electrode. A quick-drying silver paste was dripped on the backside of the SiO_2/Si substrate. Then the device was placed on a square microslide and the back-gate electrode of the FET was led to the surface of the microslide, as shown in Fig. 1a. The three electrodes of the FET are facing upwards for subsequent tests.
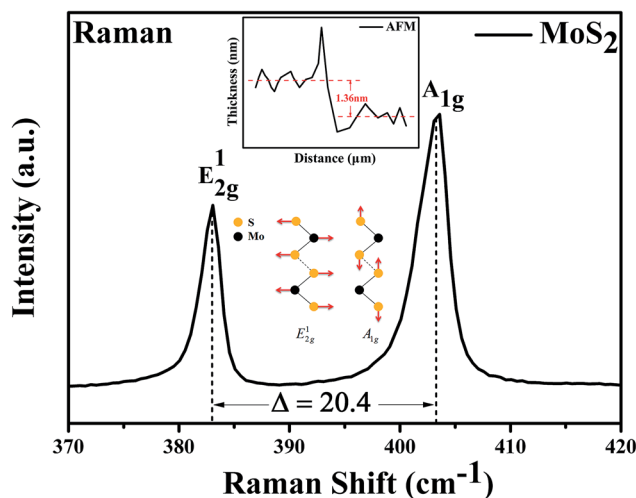

Fig. 2   Raman spectrum of the channel material. The number of layers of the MoS_2 nanosheet we prepared can be confirmed as bilayer. Inset, the height gradient between the channel material and the underlying substrate was tested by the AFM, the thickness of the MoS_2 channel material is 1.36 nm.
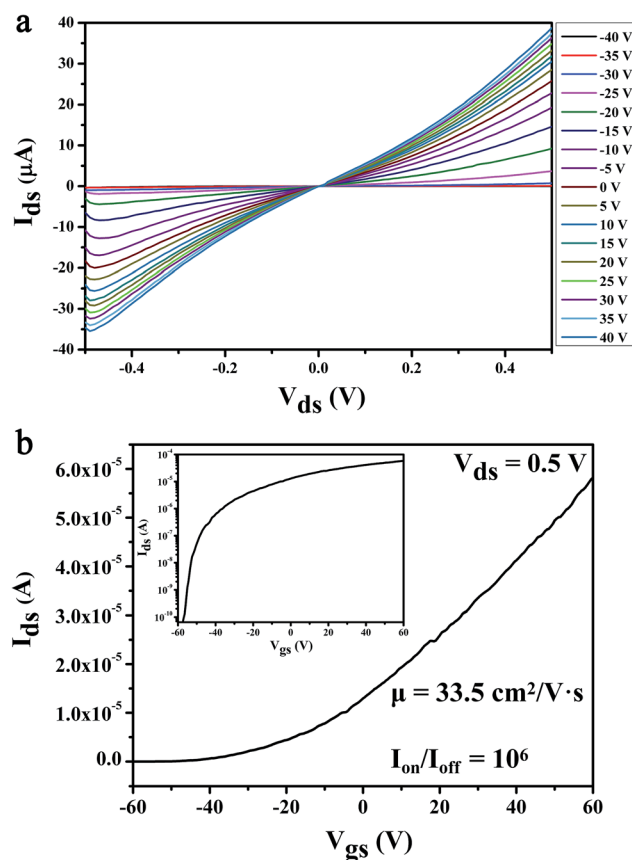

Fig. 3   The basic electrical characterization of the MoS_2 FET. (a) Output characteristic curve of the device, drain current (I_{ds}) as a function of drain voltage (V_{ds}) with the back gate voltage (V_{gs}) varying from −40 to 40 V, in a step of 5 V. (b) Transfer characteristic curve of the device, I_{ds} as a function of V_{gs} with the V_{ds} of 0.5 V. Inset, the logarithmic image of transfer characteristic curve (I_{ds}–V_{gs}).

Measurements

The thickness of the channel material (MoS$_2$ nanosheet) were tested by the atomic force microscope (AFM, Dimension 3100). And the number of layers of MoS$_2$ also been determined by measuring the Raman spectra (labRAM HR E, HORIBA) according to the shift of the in-plane vibration mode E$^1_{2g}$ and the out-plane vibration mode A$_{1g}$. Then the basic electrical characteristics of the MoS$_2$ FET without glucose solution were tested before the examination of sensing performance. A suitable device was selected as the glucose biosensor. At last, the changes of the electrical properties of biosensor with different glucose concentration were measured by the semiconductor parameter analyzer (B1500, Keysight). The data of the relationship between the I_{ds} and the glucose concentration was obtained and the sensitivity of the glucose biosensor was calculated.

Results and discussion

Basic characterization of MoS$_2$ FET

Characterization of the optical properties of the MoS$_2$ by Raman spectroscopy is not only fast and accurate, but also does not destroy the crystal structure of the sample. The number of layers of the MoS$_2$ can be determined by measuring the Raman shift of the in-plane vibration mode E$^1_{2g}$ and the out-plane vibration mode A$_{1g}$. For instance, the Raman shift of monolayer MoS$_2$ is
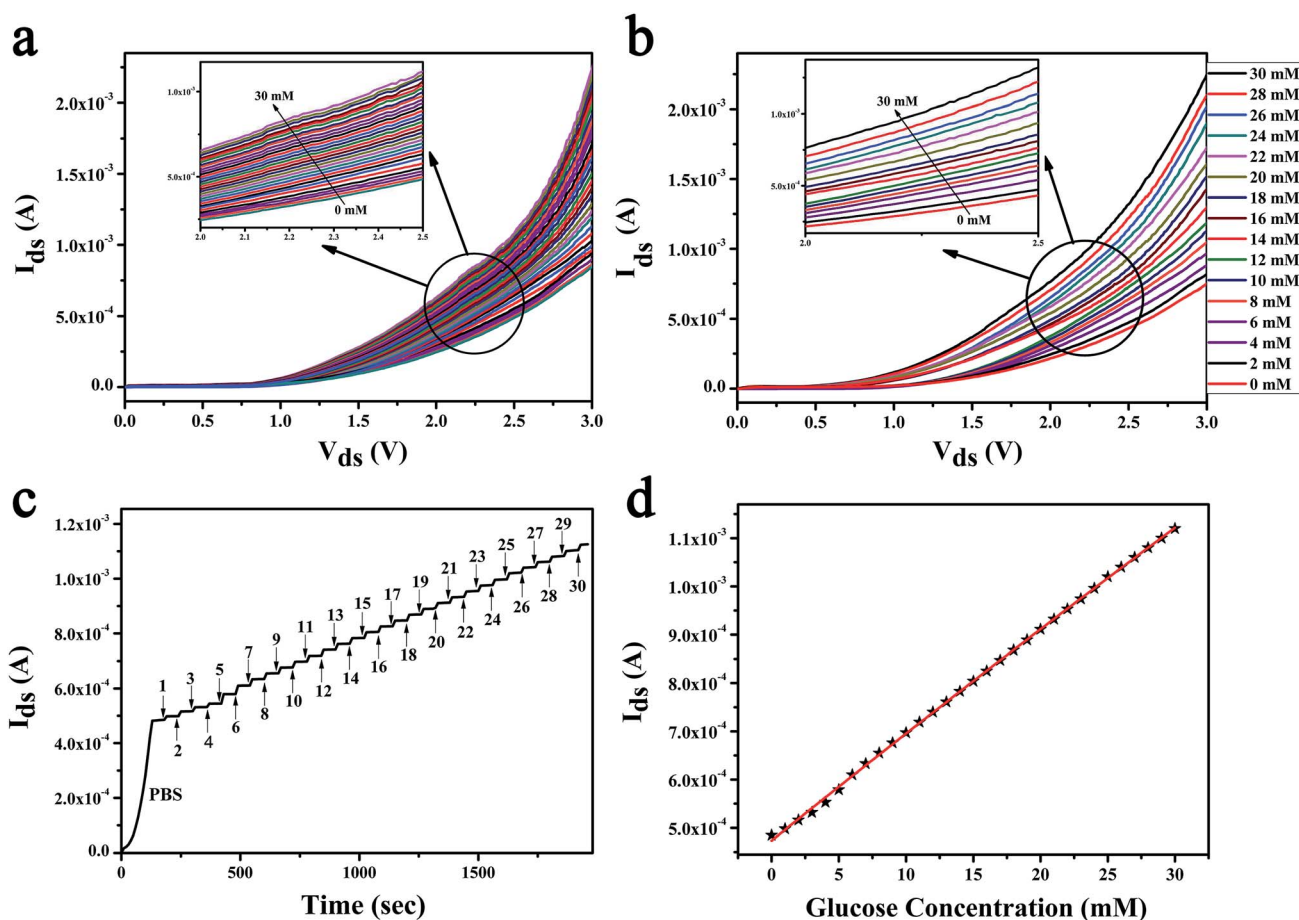

Fig. 4 MoS$_2$ FET sensor for glucose sensing. (a) Drain current for an n-type MoS$_2$ FET-based glucose sensor is plotted as a function of V_{ds} for different concentrations of the glucose solution. (b) Repeatability experiments of the glucose sensing. The even number points of glucose concentration values are tested by the device used in the (a). (c) The real time current responses to the fluctuation of glucose concentrations. The glucose responses for the sequential concentration increase at V_{gs} of 0.5 V and V_{ds} of 2.5 V. (d) The response curve of the MoS$_2$ FET to glucose solution. I_{ds} as a function of glucose concentration which is from 0 to 30 mM.

Table 1 The date of corresponding relationship between I_{ds} and glucose concentration

I_{ds} (mA)	0.498	0.516	0.532	0.553	0.579	0.610	0.633	0.655	0.676	0.697
Glucose (mM)	1	2	3	4	5	6	7	8	9	10
I_{ds} (mA)	0.719	0.740	0.761	0.783	0.804	0.825	0.847	0.868	0.889	0.911
Glucose (mM)	11	12	13	14	15	16	17	18	19	20
I_{ds} (mA)	0.932	0.953	0.974	0.996	1.021	1.043	1.062	1.084	1.107	1.129
Glucose (mM)	21	22	23	24	25	26	27	28	29	30

16–18 cm^{-1}; the Raman shift of bilayer and trilayer MoS$_2$ are 21 cm^{-1} and 23 cm^{-1}, respectively.[39–43] The testing results of Raman spectroscopy shown that the Raman shift of MoS$_2$ is 20.4 cm^{-1} with the excitation of the 532 nm laser, as shown in Fig. 2. It can be inferred that the channel material we prepared is the bilayer MoS$_2$ nanosheet. In addition, the height gradient between the channel material and the underlying substrate was tested by the AFM, as shown in Fig. 2 inset. The test results shown that the thickness of the MoS$_2$ channel material is 1.36 nm, it also validated the Raman data of the bilayer MoS$_2$ we have tested.

The electrical characteristics of the MoS$_2$ FET have a strong impact on the sensitivity of the biosensor. The testing of the electrical properties of the MoS$_2$ nanosheet based FET without glucose solution is shown in Fig. 3. As the output characteristic (I_{ds}–V_{ds}) curve shown in Fig. 3a, the I_{ds} increases with the increase of V_{ds}. Especially in the low voltage region of V_{ds}, it can be observed that the I_{ds} increases linearly with V_{ds} and the curve pass through the original point, indicating that the good ohmic contact was formed between the electrodes and MoS$_2$ layers, which is beneficial to the injection of electrons. The device can be effectively controlled by the V_{gs}, which is illustrated by the output characteristic curve of the device with different V_{gs} in Fig. 3a; several important electrical parameters of MoS$_2$ FET can be achieved from the transfer characteristic curve (I_{ds}–V_{gs}) and the logarithmic image of I_{ds}–V_{gs}, which was shown in Fig. 3b and its illustrations. According to calculation results: the field-effect mobility (μ) reached 33.5 cm^2 V^{-1} s^{-1}, the trans-conductance (g_m) was 1.7 and the switching current ratio (I_{on}/I_{off}) was as high as 10^6.

Detection of glucose using MoS$_2$ FET based biosensor

In the research of glucose sensing performance, the output characteristic curves were tested with the different glucose concentration. Fig. 4a shown the I_{ds} of MoS$_2$ FET varies with the concentration of glucose solution. This phenomenon can be explained by the enzymatic reaction of glucose with GOx and formation of the products.[44] The underlaying sensing mechanism of the glucose biosensor based on bilayer MoS$_2$ FET is attributed to the reaction of H$_2$O$_2$ generated by the oxidation of glucose. The details is that the glucose solution can generate gluconate and hydrogen peroxide (H$_2$O$_2$) after being catalyzed by the glucose oxidase (GOx), and H$_2$O$_2$ will be dissociated and produce hydrogen ions (H$^+$) and electrons (e$^-$). The concentration of electrons increases on the surface of conductive channel of the device with the process of enzymatic reaction. And the conductance of the channel material is increased because the MoS$_2$ is a n-type semiconductor. This is due to the n-doping effect resulting from the direct electron transfer on the surface of the MoS$_2$ nanosheet. There would be a charge transfer from the H$_2$O$_2$ molecules to the MoS$_2$ channel.[26,27,44–49] The glucose oxidation reaction is as follows:

$$\text{D-Glucose} + \text{H}_2\text{O} + \text{O}_2 \xrightarrow{\text{GOx}} \text{D-gluconic acid} + \text{H}_2\text{O}_2$$

$$\text{H}_2\text{O}_2 \rightarrow \text{O}_2 + 2\text{H}^+ + 2\text{e}^-$$
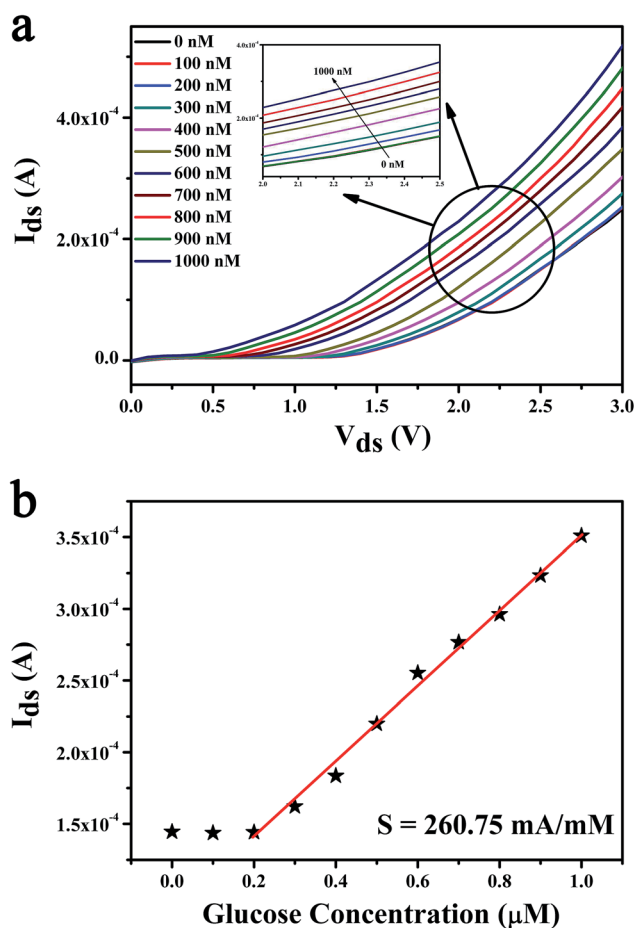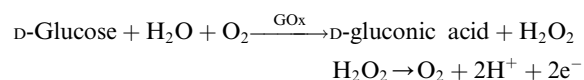
Fig. 5 MoS$_2$ FET sensor for ultra low concentration glucose sensing. (a) The detection limit of the biosensor based on MoS$_2$ FET observed by the output characteristic curve is 300 nM. (b) Drain current as a function of glucose concentration which ranges from 0 to 1 µM at V_{gs} of 0.5 V and V_{ds} of 2.5 V. By calculation, the sensitivity of our biosensor has been achieved as high as 260.75 mA mM^{-1}.

The repeatability experiments were carried out by the same device and under the same conditions after 45 days. The device was used to test the even number points of glucose concentration values, as shown in Fig. 4b. The results shown that the device has a good stability. The real time sensor response to the addition of different concentration of glucose was shown in the Fig. 4c. The test was started with a pure PBS solution under fixed V_{ds} of 2.5 V and V_{gs} of 0.5 V. 1 mM glucose solution was first injected at 180 s. And then, the glucose solution with higher concentrations were replaced the last one ever minute thereafter. The relationship between glucose concentration and the electrical parameters of MoS$_2$ FET were shown in Fig. 4d. Then the unknown concentrations of glucose solution can be detected by the I_{ds} of the MoS$_2$ FET (V_{gs} of 0.5 V, V_{ds} of 2.5 V), as illustrated in Table 1.

Sensitivity test

In order to research the detection limit and the sensitivity of the MoS$_2$ FET based biosensor, the glucose solution with extremely

Table 2 Analytical features of some reported for glucose biosensors based on the FET[a]

Modified surface	Sensitivity	LDR	DL	Response time	Reference
CPNTs	nr	0.5–20 mM	nr	5–10 s	Yoon et al. (2008)
Graphene	nr	3.3–10.9 mM	3.3 mM	nr	Kwak et al. (2012)
Graphene	0.4086 mA mM^{-1}	1.25–10 mM	1.25 mM	nr	Cagang et al. (2016)
Graphene	2.5 µA mM^{-1}	0.1–10 mM	0.1 mM	nr	You and Pak (2014)
rGO/C-PPy NT	nr	nr	1 nM	<1 s	Park et al. (2015)
SGGT	17.3 mV M^{-1}	0.5–300 µM	0.5 µM	nr	Zhang et al. (2014)
ZnO NRs	10 mA cm^{-2} mM^{-1}	0.001–45 mM	1 µM	nr	Ahmada et al. (2013)
CNTFs	0.302 mV mg^{-1} dl^{-1}	60–360 mg dl^{-1}	60 mg dL^{-1}	nr	Tsai et al. (2013)
ZnO NRs	38.9 µA mM^{-1}	800 nM to 25 mM	800 nM	nr	Lee and Chiu (2015)
ZnO	nr	1–100 µM	1 µM	<0.1 s	Ali et al. (2009)
ZnO	2.7 A mM^{-1}	10–30 mM	nr	20 s	Yano et al. (2012)
MWCNTCOOH/PAN	nr	0.005–50 mM	0.5 mM	10 s	Fathollahzadeh et al. (2016b)
Bilayer MoS$_2$	260.75 mA mM^{-1}	300 nM to 30 mM	300 nM	<1 s	Our research

[a] LDR, linear dynamic range; DL, detection limit; CPNTs, carboxylated polypyrrole nanotubes; rGO/C-PPy NT, reduced graphene oxide/carboxylated polypyrrole nanotube; SGGT, solution gated graphene transistors; ZnO NRs, ZnO nanorods; CNTFs, carbon nanotube thin films; MWCNTCOOH/PAN, multi-walled carbon nanotubes-polyaniline nanocomposite; nr, not reported.

low concentration which from 0 nM to 1 µM was detected by the change of output characteristic curves, as shown in Fig. 5a.

The detection limit of our biosensor is 300 nM. The I_{ds} as a function of glucose concentration was shown in Fig. 5b. The sensitivity of the glucose biosensor can be calculated as high as 260.75 mA mM^{-1}. And the response time (<1 s) and the linear regions (300 nM to 30 mM) were tested in our experiments. Analytical features of some reported for glucose biosensors based on the FET are summarized in the Table 2 and compared with those parameters obtained from our results using bilayer MoS$_2$ FET. As shown in Table 2, the proposed ZnO-based glucose biosensor shown higher sensitivity,[28] shorter response time[45] and wider linear dynamic range[50] than those previous reports.[26,27,46,47,51–55] And the detection limit of the reduced graphene oxide/carboxylated polypyrrole nanotube (rGO/C-PPy NT) FET based biosensor[42] was better than other glucose biosensors.[26–28,45–47,50–55] Compared with previous researches, the bilayer MoS$_2$-based FET we prepared show significant advantages in high sensitivity detection of extremely low concentration glucose solution.

Conclusions

In summary, a biosensor based on the bilayer MoS$_2$ back-gate FET was fabricated and demonstrated for glucose detection successfully in our research. In particular, the glucose concentration was detected by the MoS$_2$ FET for the first time. Considering the concentration of the fasting blood ranges from 3.9 to 6.1 mM, the concentration was detected in the range of 0–30 mM by the glucose biosensor we prepared. Through measurements of the I_{ds}, the fabricated MoS$_2$ FET biosensor shown a good sensing performance. The high sensitivity of 260.75 mA mM^{-1} was achieved for the detection of glucose solution which has the extremely low concentration level (300 nM). The other advantages of our biosensor such as short response time (<1 s), good stability, small size and trace detection were all demonstrated in our studies. This article open up

a new path for the applications about the MoS$_2$ FET. In practical sensing applications, we can design a bio-integrated circuit which contains a FET, an operational amplifier, a comparator and an LED to achieve the macroscopic, fast detection. That can be used to realize the miniaturization and real-time detection of human blood glucose concentration in the future.

Conflicts of interest

There are no conflicts to declare.

Acknowledgements

References

1 D. Lembke, S. Bertolazzi and A. Kis, *Acc. Chem. Res.*, 2015, **48**, 100–110.
2 D. Krasnozhon, D. Lembke, C. Nyffeler, Y. Leblebici and A. Kis, *Nano Lett.*, 2014, **14**, 5905–5911.
3 K. F. Mak, C. Lee, J. Hone, J. Shan and T. F. Heinz, *Phys. Rev. Lett.*, 2010, **105**, 136805.
4 W. X. Gu, J. Y. Shen and X. Y. Ma, *Nanoscale Res. Lett.*, 2014, **9**, 100.
5 T. Kawanago and S. Oda, *Appl. Phys. Lett.*, 2016, **108**, 041605.
6 Y. Chen, X. D. Wang, P. Wang, H. Huang, G. J. Wu, B. Tian, Z. C. Hong, Y. T. Wang, S. Sun, H. Sheng, J. L. Wang, W. D. Hu, J. L. Sun, X. J. Meng and J. H. Chu, *ACS Appl. Mater. Interfaces*, 2016, **8**, 32083–32088.

7 D. J. Late, B. Liu, H. S. S. R. Matte, V. P. Dravid and C. N. R. Rao, *ACS Nano*, 2012, **6**, 5635–5641.

8 D. Jariwala, V. K. Sangwan, D. J. Late, J. E. Johns, V. P. Dravid, T. J. Marks, L. J. Lauhon and M. C. Hersam, *Appl. Phys. Lett.*, 2013, **102**, 173107.

9 P. K. Kannan, D. J. Late, H. Morgan and C. S. Rout, *Nanoscale*, 2015, **7**, 13293–13312.

10 D. J. Late, P. A. Shaikh, R. Khare, R. V. Kashid, M. Chaudhary, M. A. More and S. B. Ogale, *ACS Appl. Mater. Interfaces*, 2014, **6**, 15881–15888.

11 D. Sarkar, W. Liu, X. J. Xie, A. C. Anselmo, S. Mitragotri and K. Banerjee, *ACS Nano*, 2014, **4**, 3992–4003.

12 W. Yang, K. R. Ratinac, S. P. Ringer, P. Thordarson, J. J. Gooding and F. Braet, *Angew. Chem., Int. Ed.*, 2010, **49**, 2114–2138.

13 M. S. Makowski and A. Ivanisevic, *Small*, 2011, **7**(14), 1863–1875.

14 Y. Ohno, K. Maehashi, Y. Yamashiro and K. Matsumoto, *Nano Lett.*, 2009, (9), 3318–3322.

15 Y. Ohno, K. Maehashi and K. Matsumoto, *J. Am. Chem. Soc.*, 2010, **132**, 18012–18013.

16 M. Dankerl, M. V. Hauf, A. Lippert, L. H. Hess, S. Birner, I. D. Sharp, A. Mahmood, P. Mallet, J. Y. Veuillen, M. Stutzmann and J. A. Garrido, *Adv. Funct. Mater.*, 2010, **20**, 3117–3124.

17 D. J. Late, Y. K. Huang, B. Liu, J. Acharya, S. N. Shirodkar, J. J. Luo, A. Yan, D. Charles, U. V. Waghmare, V. P. Dravid and C. N. R. Rao, *ACS Nano*, 2013, **7**, 4879–4891.

18 G. Yoo, H. Park, M. Kim, W. G. Song, S. Jeong, M. H. Kim, H. Lee, S. W. Lee, Y. K. Hong, M. G. Lee, S. Lee and S. Kim, *Nano Res.*, 2017, **10**(3), 767–775.

19 B. Liu, L. Chen, G. Liu, A. N. Abbas, M. Fathi and C. Zhou, *ACS Nano*, 2014, **8**, 5304–5314.

20 J. W. Huang, Y. Q. He, J. Jin, Y. R. Li, Z. P. Dong and R. Li, *Electrochim. Acta*, 2014, **136**, 41–46.

21 J. W. Huang, Z. P. Dong, Y. D. Li, J. Li, J. Wang, H. D. Yang, S. W. Li, S. J. Guo, J. Jin and R. Li, *Sens. Actuators, B*, 2013, **182**, 618–624.

22 X. Y. Li and X. Z. Du, *Sens. Actuators, B*, 2017, **239**, 536–543.

23 L. M. Lu, H. B. Li, F. L. Qu, X. B. Zhang, G. L. Shen and R. Q. Yu, *Biosens. Bioelectron.*, 2011, **26**, 3500–3504.

24 K. I. Ozoemena and T. Nyokong, *Electrochim. Acta*, 2006, **51**, 5131–5136.

25 Y. Y. Su, B. B. Luo and J. Z. Zhang, *Anal. Chem.*, 2016, **88**, 1617–1624.

26 Y. H. Kwak, D. S. Choi, Y. N. Kim, H. Kim, D. H. Yoon, S. S. Ahn, J. W. Yang, W. S. Yang and S. Seo, *Biosens. Bioelectron.*, 2012, **37**, 82–87.

27 H. Yoon, S. Ko and J. Jang, *J. Phys. Chem. B*, 2008, **112**, 9992–9997.

28 M. Yano, K. Koike, K. Ogata, T. Nogami, S. Tanabe and S. Sasa, *Phys. Status Solidi*, 2012, **9**, 1570–1573.

29 Y. M. Lin, K. A. Jenkins, A. Valdes-Garcia, J. P. Small, D. B. Farmer and P. Avouris, *Nano Lett.*, 2008, **9**, 422–426.

30 P. Wei, N. Liu, H. R. Lee, E. Adijanto, L. Ci, B. D. Nabb, J. Q. Zhong, J. Park, W. Chen, Y. Cui and Z. Bao, *Nano Lett.*, 2013, **13**, 1890–1897.

31 Y. M. Lin, C. Dimitrakopoulos, K. A. Jenkins, D. B. Farmer, H. Y. Chiu, A. Grill and P. Avouris, *Science*, 2010, **327**, 662.

32 S. Lebegue and O. Eriksson, *Phys. Rev. B: Condens. Matter Mater. Phys.*, 2009, **79**, 115409.

33 A. Splendiani, L. Sun, Y. Zhang and F. Wang, *Nano Lett.*, 2010, **10**, 1271.

34 A. Kuc, N. Zibouche and T. Heine, *Phys. Rev. B: Condens. Matter Mater. Phys.*, 2011, **83**, 245213.

35 S. L. Li, K. Komatsu, S. Nakaharai, Y. F. Lin, M. Yamamoto, X. F. Duan and K. Tsukagonshi, *ACS Nano*, 2014, 12836–12842.

36 S. Kim, A. Konar, W. S. Hwang, J. H. Lee, J. Lee, J. Yang, C. Jung, H. Kim, J. Yoo, J. Y. Choi, Y. W. Jin, S. Y. Lee, D. Jena, W. Choi and K. Kim, *Nat. Commun.*, 2012, **20**, 1038.

37 B. W. H. Baugher, H. O. H. Churchill, Y. Yang and P. J. Herrero, *Nano Lett.*, 2013, **13**, 4212–4216.

38 H. Li, Z. Y. Yin, Q. Y. He, H. Li, X. Huang, G. Lu, D. W. H. Fam, A. L. Y. Tok, Q. Zhang and H. Zhang, *Small*, 2012, **8**, 63–67.

39 A. S. Pawbake, M. S. Pawar, S. R. Jadkar and D. J. Late, *Nanoscale*, 2016, **8**, 3008–3018.

40 M. X. Ye, D. Winslow, D. Y. Zhang, R. Pandey and Y. K. Yap, *Photonics*, 2015, **2**, 288–307.

41 S. Tongay, W. Fan, J. Kang, J. Park, U. Koldemir, J. Suh, D. S. Narang, K. Liu, J. Ji, J. Li, R. Sinclair and J. Wu, *Nano Lett.*, 2014, **14**, 3185.

42 X. Li, J. H. Li, X. H. Wang, J. X. Hu, X. Fang, X. Y. Chu, Z. P. Wei and J. J. Shan, *Integr. Ferroelectr.*, 2014, **158**, 26–42.

43 C. G. Lee, H. G. Yan, L. E. Brus, T. F. Heinz, J. Hone and S. Ryu, *ACS Nano*, 2010, **5**, 2695–2700.

44 M. Fathollahzadeh, M. Hosseini, B. Haghighi and M. Fathipour, *Anal. Chim. Acta*, 2016, **924**, 99–105.

45 R. Ahmad, N. Tripathy and Y. B. Hahn, *Biosens. Bioelectron.*, 2013, **45**, 281–286.

46 M. Zhang, C. Z. Liao, C. H. Mak, P. You, C. L. Mak and F. Yan, *Sci. Rep.*, 2015, **5**, 8311.

47 W. L. Tsai, Y. S. Chien, P. Y. Yang, I. C. Lee, K. Y. Wang and H. C. Cheng, *Sens. Actuators, A*, 2013, **204**, 31–36.

48 Y. H. Lin, C. P. Chu, C. F. Lin, H. H. Liao, H. H. Tsai and Y. Z. Juang, *Biomed. Microdevices*, 2015, **17**, 111.

49 X. You and J. J. Pak, *Sens. Actuators, B*, 2014, **202**, 1357–1365.

50 S. M. U. Ali, O. Nur, M. Willander and B. Danielsson, *IIEEE Trans. Nanotechnol.*, 2009, **6**, 678–683.

51 A. A. Cagang, I. H. Abidi, A. Tyagi, J. Hu, F. Xu, T. J. Lu and Z. Luo, *Anal. Chim. Acta*, 2016, **917**, 101–106.

52 X. Q. You and J. J. Pak, *Sens. Actuators, B*, 2014, **202**, 1357–1365.

53 J. W. Park, C. Lee and J. Jang, *Sens. Actuators, B*, 2015, **208**, 532–537.

54 C. T. Lee and Y. S. Chiu, *Sens. Actuators, B*, 2015, **210**, 756–761.

55 M. Fathollahzadeh, M. Hosseini, B. Haghighi, M. Kolahdouz and M. Fathipour, *Anal. Chim. Acta*, 2016, **924**, 99–105.